Anal. Chem. **2002,** *74,* 4311−4319

Accelerated Articles

Confocal Raman Microscopy for Monitoring Chemical Reactions on Single Optically Trapped, Solid-Phase Support Particles

Michael P. Houlne, Christopher M. Sjostrom, Rory H. Uibel, James A. Kleimeyer, and Joel M. Harris*

Department of Chemistry, University of Utah, 315 South 1400 East, Salt Lake City, Utah 84112-0850

Optical trapping of small structures is a powerful tool for the manipulation and investigation of colloidal and particulate materials. The tight focus excitation requirements of optical trapping are well suited to confocal Raman microscopy. In this work, an inverted confocal Raman microscope is developed for studies of chemical reactions on single, optically trapped particles and applied to reactions used in solid-phase peptide synthesis. Optical trapping and levitation allow a particle to be moved away from the coverslip and into solution, avoiding fluorescence interference from the coverslip. More importantly, diffusion of reagents into the particle is not inhibited by a surface, so that reaction conditions mimic those of particles dispersed in solution. Optical trapping and levitation also maintain optical alignment, since the particle is centered laterally along the optical axis and within the focal plane of the objective, where both optical forces and light collection are maximized. Hour-long observations of chemical reactions on individual, trapped silica particles are reported. Using two-dimensional least-squares analysis methods, the Raman spectra collected during the course of a reaction can be resolved into component contributions. The resolved spectra of the time-varying species can be observed, as they bind to or cleave from the particle surface.

Optical trapping of small structures, based on radiation pressure from a strong intensity gradient defined by a tight laser focus or "laser tweezers",[1−3] is a powerful tool[4] for the manipulation and investigation of biological cells,[5−8] vesicles,[8−10] and inorganic and organic colloids.[1,11−13] Tight focus excitation requirements of optical trapping are well suited to Raman microscopy. The first experiments combining optical trapping with Raman scattering measurements were applied to levitation and trapping of micrometer-sized solid particles,[14] liquid droplets,[15] and photopolymerizing aerosols[16] in the gas phase. More recently, single micrometer-sized droplets of organic liquids in aqueous emulsions have been trapped and examined by Raman spectroscopy.[17,18] This technique has also been applied to Raman studies of polymerization reactions in single emulsion particles[19] and photoinduced changes in the conjugation of trapped polystyrene particles.[20] Confocal Raman microscopy,[21−23] where matched excitation/collection volumes are

* Corresponding author. E-mail: harrisj@chemistry.chem.utah.edu.

(1) Ashkin, A.; Dziedzic, J. M.; Bjorkholm, J. E.; Chu, S. *Opt. Lett.* **1986**, *11*, 288−90.
(2) Wright, W. H.; Sonek; G. J.; Berns, M. W. *Appl. Phys. Lett.* **1993**, *63*, 715−17.
(3) Askin, A. Proc. *Natl. Acad. Sci. U.S.A.* **1997**, *94*, 4853−4860.
(4) Ashkin, A. *IEEE J. Sel. Top. Quantum Electron.* **2000**, *6*, 841−856.
(5) Askin, A.; Dziedzic, J. M. *Science* **1987**, *235*, 1517−1520.
(6) Liu, Y.; Sonek, G. J.; Berns, M. W.; Tromberg, B. J. *Biophys. J.* **1996**, *71*, 2158−2167.
(7) Wei, X.; Tromberg, B. J.; Cahalan, M. D. *Proc. Natl. Acad. Sci. U.S.A.* **1999**, *96*, 8471−8476.
(8) Strömberg, A.; Karlsson, A.; Ryttsén, F.; Davidson, M.; Chiu, D. T.; Owar, O. *Anal. Chem.* **2001**, *73*, 126−130.
(9) Chiu, D. T.; Hsaio, A.; Gaggar, A.; Garza-López, R. A.; Owar, O.; Zare, R. N. *Anal. Chem.* **1997**, *69*, 1801−1807.
(10) Chiu, D. T.; Lillard, S. J.; Scheller, R. H.; Zare, R. N.; Rodriguez-Cruz, S. E.; Williams, E. R.; Orwar, O.; Sandberg, M.; Lundqvist, J. A. *Science* **1998**, *279*, 1190−1193.
(11) Clapp, A. R.; Ruta, A. G.; Dickinson, R. B. *Rev. Sci. Instrum.* **1999**, *70*, 2627−2636.
(12) Viravathana, P.; Marr, D. W. M. *J. Colloid Interface Sci.* **2000**, *221*, 301−307.
(13) Mio, C.; Marr, D. W. M. *Adv. Mater.* **2000**, *12*, 917−920.
(14) Thurn, R.; Kiefer, W. *Appl. Spectrosc.* **1984**, *38*, 78−83.
(15) Thurn, R.; Kiefer, W. *Appl. Opt.* **1985**, *24*, 1515−1519.
(16) Esen, C.; Kaiser, T.; Schweiger, G. *Appl. Spectrosc.* **1996**, *50*, 823−828.
(17) Lankers, J.; Popp, J.; Kiefer, W. *Appl. Spectrosc.* **1994**, *48*, 1166−1168.
(18) Ajito, K. *Appl. Spectrosc.* **1998**, *52*, 339−342.
(19) Urlaub, E.; Lankers, M.; Hartmann, I.; Popp, J.; Trunk, M.; Kiefer, W. *Chem. Phys. Lett.* **1994**, *231*, 511−514.
(20) Crawford, K. D.; Hughes, K. D. *J. Phys. Chem. B* **1998**, *102*, 2325−2328.

10.1021/ac020325t CCC: $22.00
Published on Web 07/24/2002

defined by imaging through an aperture, is a powerful method for optimizing the collection of scattering from a localized volume in the sample while minimizing the background from the surrounding material. Confocal Raman microscopy has been combined recently with optical trapping in an upright microscope to detect 15-μm toluene droplets and submicrometer polystyrene particles.[18,24]

In the present work, an inverted confocal Raman microscope is developed for studies of chemical reactions on single, optically trapped particles and applied to reactions used in solid-phase synthesis. The inverted configuration allows particles to be captured and levitated from the surface of the coverslip where they settle. It also places the sample cell above the objective, providing convenient access for changing solution composition and initiating chemical reactions. High numerical aperture (1.4 NA), oil immersion optics, and the confocal excitation/collection design provide high throughput, low background, and submicrometer spatial resolution. Long-wavelength (647 nm) excitation avoids the photochemical damage reported previously at shorter wavelengths.[20,25]

Solid-phase synthesis is becoming a common strategy in the pharmaceutical and biotechnology industries for generating molecular libraries for high-throughput screening.[26,27] The popularity of solid-phase reaction schemes over traditional solution-phase methods has arisen mainly because these schemes require smaller quantities of reagents and the final product can be easily separated and isolated from the reaction mixture. Despite these advantages of solid-phase synthesis over solution-phase methods, a lack in understanding of the surface chemistry of the substrates, their effects on reaction kinetics, and particle-to-particle variation in reactivity can hinder progress in understanding and developing solid-phase reaction schemes. Traditional analytical methods are not practical for monitoring the progress of these reactions or measuring their kinetics. For example, many analytical techniques such as mass spectrometry and chromatography (HPLC, TLC, GC) can only be used ex situ and require an additional chemical step to cleave the product from the solid support. Typically these techniques also require large quantities of sample and experiment time. These limitations call for an on-line, in situ detection method that can be performed on the time scale of the solid-phase chemical reactions.

Several investigators have explored the use infrared and NIR spectroscopies has as potential tools for monitoring of solid-phase reactions.[27−36] For example, Fischer and Tran[33] recently showed that NIR imaging can be used to follow several solid-phase reactions simultaneously in multiple wells. Huber and co-workers[34] demonstrated the use of ATR FT-IR microscopy to verify product structure and reaction completeness on a single polystyrene bead during a reaction sequence. Regardless of the detection technique employed, both near-IR and ATR FT-IR are amendable for in situ analysis since no additional sample preparation is required, thus reducing analysis time and minimizing reagent use.

Raman spectroscopy has also been investigated as an alternative vibrational spectroscopy for these reactions.[29,36] In a study comparing infrared and Raman spectroscopy for this application, Yan and co-workers[29] showed that Raman scattering provided complimentary information, especially for functional groups with symmetric vibrations such as NO_2, S−S, and C−halogen. Most recently, Pivonka and Sparks[36] evaluated Raman scattering for monitoring a multistep synthesis and concluded that this technique can provide real-time information about a variety of synthetic reactions and is especially useful for reactions in polar solvents that are incompatible with infrared spectroscopy.[36] Both groups concluded that the low sensitivity of Raman scattering did not make it an attractive technique for single-particle analysis.

Spatially resolved, single-particle experiments are well suited to probe the chemistry of solid-phase reactions since they selectively probe the chemistry of the particle and not the bulk reagents and solvent in the particle surroundings. In addition, they can be employed to study kinetic steps in combinatorial synthesis where variation in reaction precursors can change the kinetics of subsequent addition or deprotection steps. In the present work, we set out to demonstrate that confocal Raman microscopy can be combined with optical trapping to provide a highly sensitive method to monitor the reaction kinetics of solid-phase peptide synthesis steps. We employ optical trapping and levitation to move the particle away from the coverslip and into the solution to avoid fluorescence interferences from the coverslip. More importantly, the diffusion of reagents into the particle is not inhibited by a surface, so that reaction conditions will mimic those of particles dispersed in solution. Optical trapping and levitation are also advantageous for maintaining optimum alignment, since the particle remains centered laterally along the optical axis and within the focal plane of the objective, where both optical forces and light collection are maximized.

EXPERIMENTAL SECTION

Confocal Raman Microscope. A block diagram of the microscope optics is shown in Figure 1. The excitation source was a Kr^+ laser (Innova 90, Coherent Inc.) operating at 647.1 nm with an output power of 25 mW. The laser beam was directed by a series of mirrors through a 4× beam expander (model 50-25-4X-647, Special Optics, Inc.) mounted in the back of a Nikon TE 300 inverted fluorescence microscope. The expanded beam passed through the rear aperture of the TE 300 into a cubic housing that held a band-pass filter (D647/10, Chroma Tech, Inc.), a dichroic beam splitter (655DCLP, Chroma Tech, Inc.), and a high-pass filter

(21) Puppels, G. J.; Colier, W.; Olminkhof, J. H. F.; Otto, C.; De Mul, F. F. M.; Greve, J. *J. Raman Spectrosc.* **1991**, *22*, 217−225.
(22) Williams, K. P.; Pitt, G. D.; Batchelder, D. N.; Kip, B. J. *Appl. Spectrosc.* **1994**, *48*, 232−235.
(23) Schrum, K. F.; Seung, H. K.; Ben-Amotz, D. *Appl. Spectrosc.* **1996**, *50*, 1150−1155.
(24) Ajito, K.; Torimitsu, K. *Appl. Spectrosc.* **2002**, *56*, 541−544.
(25) Crawford, K. D.; Hughes, K. D. *J. Phys. Chem. B* **1998**, *101*, 864−870.
(26) Wilson, S. R.; Czarnik, A. W. *Combinatorial Chemistry: Synthesis and Application*; John Wiley: New York, 1997.
(27) Lam, K. S.; Lebl, M.; Krchnak, V. *Chem. Rev.* **1997**, *97*, 411−448.
(28) Czarnik, A. *Anal. Chem.* **1998**, *70*, 378A−386A.
(29) Yan, B.; Gremlich, H.; Moss, S.; Coppola, G. M.; Sun, Q.; Liu, L. *J. Comb. Chem.* **1999**, *1*, 46−54.
(30) Dolle, R. E. *J. Comb. Chem.* **2000**, *2*, 383−433.
(31) Yan, B.; Kumaravel, G.; Anjaria, H.; Wu, A.; Petter, R. C.; Jewell, C. F.; Wareing, J. R. *J. Org. Chem.* **1995**, *60*, 5736−5738.
(32) Yan, B. *Acc. Chem. Res.* **1998**, *31*, 621−630.
(33) Fischer, M.; Tran, C. D. *Anal. Chem.* **1999**, *71*, 2255−2261.
(34) Huber, H.; Bubendorf, A.; Grieder, A.; Obrecht, D. *Anal. Chim. Acta* **1999**, *393* (1−3), 213−221.
(35) Yan, B. *Analytical Methods in Combinatorial Chemistry*; Technomic Publishing Co., Inc.: Lancaster, PA, 2000 and references therein.
(36) Pivonka, D. E.; Sparks, R. B. *Appl. Spectrosc.* **2000**, *54* (11), 1584−1590.

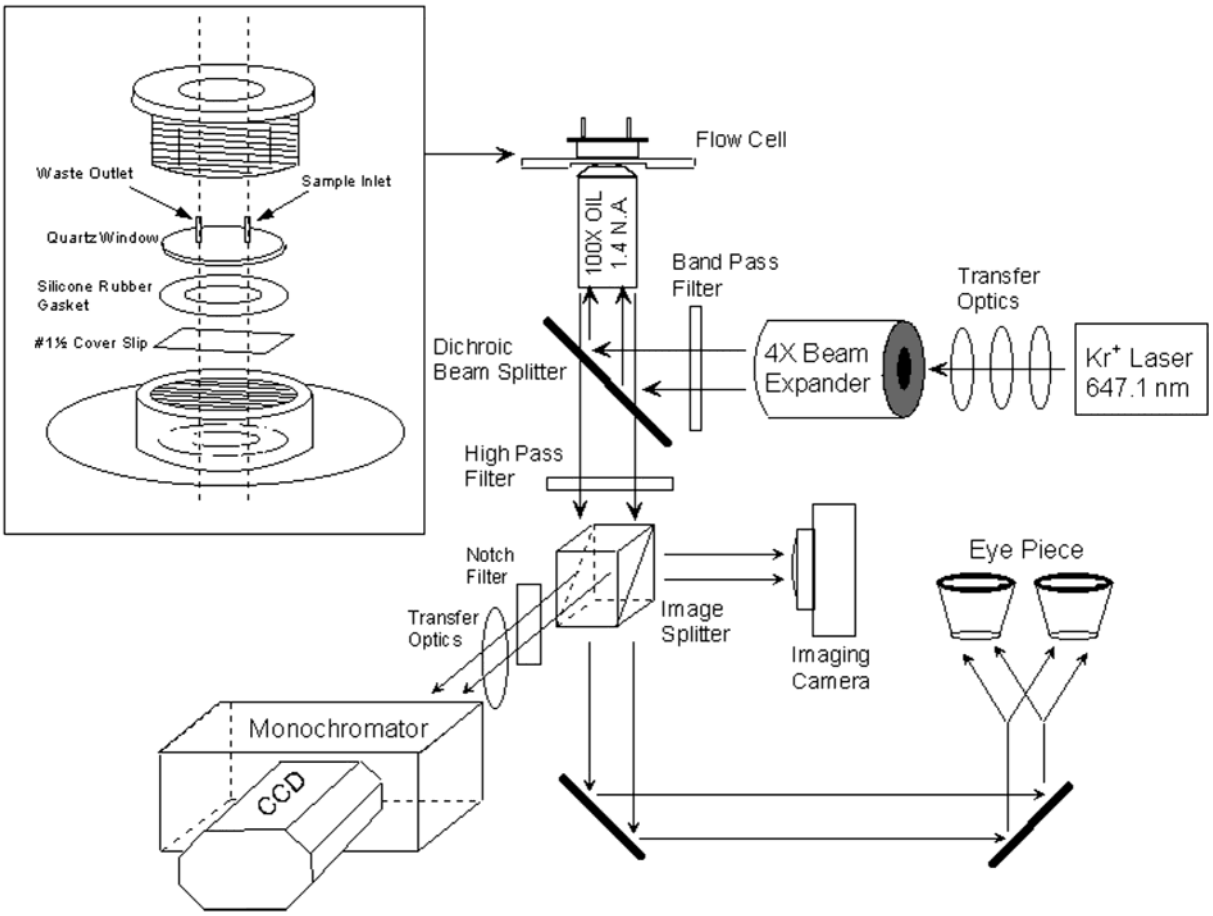

Figure 1. Block diagram of the confocal Raman microscope. A diagram of the sample flow cell is shown in the inset figure.

(E660LP, Chroma Tech, Inc.). Excitation light (16 mW) from the cube was passed through the rear aperture of a 100×, 1.4 NA oil immersion microscope objective (CFL PLAN APO, Nikon Inc.) where it was focused through a $1^1/_2$-thickness coverslip (BK-7 glass, Esco) to a 0.4-μm-diameter spot in the sample. Raman scattering from single trapped particles was collected by the same objective and focused back through the dichroic and long-pass filter and down into the body of the microscope. The image was directed to either a 10× eyepiece for visual observation, a monochromator (250IS, Chromex, Inc.) and CCD (DV420, Andor, Inc.) for spectral analysis, or a digital camera (CoolPix 950, Nikon, Inc.) for imaging. Bright-field illumination from a 0.52 NA overhead lamp assembly was employed for acquiring images of trapped particles.

A microscopy flow cell, to contain particle suspensions, was constructed from a flat silicone rubber gasket set between the coverslip and a round, quartz disk that defines a sample volume of 650 μL. This assembly, depicted in the inset of Figure 1, was housed in a cylindrical, aluminum mount that could be screwed down to evenly compress the gasket and seal the cell. The aluminum mount was fixed to the microscope stage and kept the coverslip flat with respect to the objective surface. The quartz top was fashioned with an inlet and outlet port to allow filling of the cell and also served as an illumination window for viewing and white light imaging. A specialty, low-fluorescence, immersion oil (code 510, Cargille, Inc.) was employed to minimize background.

A confocal volume for light collection was achieved by creating a square aperture in the image, using the entrance slit of the monochromator to define the horizontal limit and a small number of binned pixels in the CCD image to define the vertical axis. Using this approach previously developed by Williams et al.,[22] the monochromator slit was adjusted to 50 μm to define a 500-nm horizontal range within the sample (100× magnification) while three rows of the CCD (66 μm) were sampled to yield a 660-nm vertical range in the sample. This confocal aperture corresponds to a confocal probe volume of ~2 fL, considering the depth of field of the objective (0.5 μm[37]) and the divergence of the laser beam near its waist.[38]

Particle Preparation and Reagents. Silica particles (Lichrosorb Si-60, 5-μm particles, 60-Å pore diameter, 500 m^2/g specific surface area, 1 mL/g pore volume (EM Separations, CAS 63231-67-4)) were first dried at 30 mTorr for 24 h. The surface of the dried particles was primed with propylamine groups by suspending $2^1/_2$ g in 75 mL of dry toluene (99.9%, EM Scientific, CAS 108-88-3) and 350 μL of (3-aminopropyl)trimethoxysilane (Fluka, 09326) under a nitrogen atmosphere and stirring the resultant mixture at 35 °C for 24 h. The particles were isolated as a pellet by centrifugation (2400 rpm for 4 min) and washed with toluene. This washing process was performed four times with toluene followed by four washes with methanol. Finally, the aminated silica was dried under vacuum for 6 h, and the presence of primary amine groups was checked by a ninhydrin test. This procedure yields a coverage of 0.4 mmol/g silica based on elemental analysis (MHW Labs, Phoenix, AZ).

(37) Carlsson, K.; Åslund, N. *Appl. Opt.* **1987**, *26*, 3232−3238.
(38) Hill, E. K.; de Mello, A. J. *Analyst* **2000**, *125*, 1033−1036.

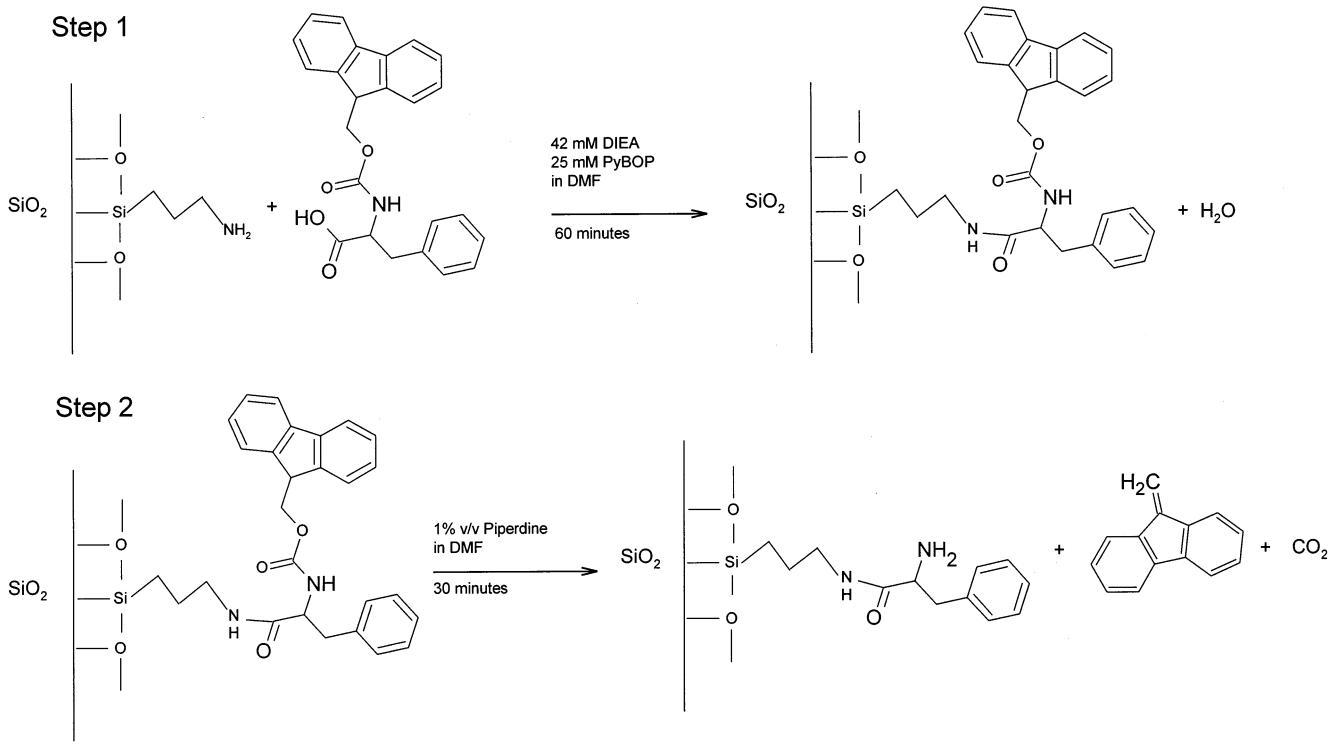

Figure 2. Synthetic scheme for fmoc-phenylalanine addition to a propylamine-primed silica surface and deprotection of the phenylalanine by removal of the Fmoc group.

The reaction scheme, depicted in Figure 2, is a simple, two-step addition and removal process developed by Welch and co-workers[39] for preparing peptide stationary phases on silica for chiral separations. In the fmoc-phenylalanine addition step, all reactants were prepared in separate vessels at initial concentrations of 0.15 M in dimethylformamide (DMF, 99.9%, Acros). For the addition reaction, diisopropylethylamine (DIEA) was obtained from Lancaster at 99% purity and the *N*-α-fmoc-L-phenylalanine (Fmoc-Phe) and benzotriazole-1-yloxytrispyrrolidinophosphonium hexafluorophosphate (PyBOP) were both obtained from Novabiochem at ≥98% purity. For the fmoc-removal step, piperdine (Sigma, 99.9%) was prepared in DMF at an initial concentration of 2 vol %.

Monitoring Single-Particle Reaction Kinetics. For both the addition and deprotection reactions, particle suspensions were initially prepared in DMF at a concentration of ∼5 μg/mL, corresponding to ∼37 000 particles/mL. A 250-μL sample of this suspension was rapidly mixed with a comparable volume of reagent for the reaction, and the reacting suspension was immediately injected into the flow cell on the microscope stage where 5−10 particles were observed within the microscope field of view. A single particle was trapped and levitated 50 μm above the coverslip surface for analysis. The time delay between mixing the particles with reagent and the acquisition of the first spectrum of the particle averaged ∼3 min.

For the fmoc-Phe addition reaction, a 250-μL sample of the particle suspension was mixed with 150 μL of the DIEA solution, 250 μL of PyBOP, and 250 μL of the Fmoc-Phe reagent (where the final concentrations are listed in Figure 2). Raman spectra (30-s integrations) were collected on the trapped particle every 2 min for 1 h. For removal of the fmoc protecting group, a 250-μL sample of the particle suspension in DMF was mixed with an equal volume of a 2% solution of piperdine in DMF. This reaction occurs on a faster time scale, and Raman spectra (30-s exposures) were collected every 90 s for 30 min.

Data Analysis. The time-dependent Raman spectra of levitated and trapped silica particles were collected into a data matrix, **D**, where the row index is the frequency in wavenumbers and the column index is the time of observation. To observe changes in band intensity due to accumulation or loss of molecules on the silica surface, the spectra were corrected for background from solution-phase components. Due to the porous nature of the particles, a significant fraction of the particle volume (1 mL/g) consists of intraparticle solution filling the pores. Since the volume of solution sampled in the presence of the particle is less than in free solution, background spectra in the absence of a particle were scaled to match the fraction of solution intensity in the particle spectra. The intensity of the strongest DMF solvent band at 825 cm^{-1} was chosen to scale the background subtraction.

Multidimensional least-squares analysis was used to resolve the spectra in **D** into spectra of components in the sample and also to determine the rate of accumulation or loss of molecules in the particle. At a given wavenumber, the Raman scattering intensity of a mixture of species can be expressed as a sum of each contribution to the total scattering intensity:

$$d_{ij} = \sum_{k=1}^{n} a_{ik} c_{kj} \qquad (1)$$

where a_{ik} represents the Raman spectrum of the kth component

(39) Welch, C. J.; Bhat, G.; Protopopova, M. N. *Enantiomer* **1998**, *3* (6), 463−469.

at wavenumber i and c_{kj} indicates the concentration of component at the jth time interval. The relationship in eq 1 can be expressed as a matrix product:

$$\mathbf{D} = \mathbf{AC} \tag{2}$$

where **A** is a column matrix containing the Raman spectra of species in the mixture and **C** is a row matrix comprising the time-dependent concentration profiles for each component in **A**.

Assuming a model for the reaction kinetics can be constructed for **C**, a least-squares estimate of the component spectra can be determined:[40]

$$\hat{\mathbf{A}} = \mathbf{DC}^{\mathbf{T}}(\mathbf{CC}^{\mathbf{T}})^{-1} \tag{3}$$

From the estimated component spectra, $\hat{\mathbf{A}}$, a model for the data, $\hat{\mathbf{A}}\mathbf{C}$, leads to an esimate of the residual error **R**:

$$\mathbf{R} = \mathbf{D} - \hat{\mathbf{A}}\mathbf{C} \tag{4}$$

where each element r_{ij} is the difference between the data set and the data reconstructed from the estimated matrix $\hat{\mathbf{A}}$ via eq 2. The model used for **C** often contains an unknown parameter (e.g., the reaction rate constant). A nonlinear least-squares method approach can be employed to optimize these parameters,[41,42] where a global error surface defined by **R** is determined for combinations of the nonlinear parameters used to define **C**, where eqs 3 and 4 are computed at each step until the sum of the squared residual error χ^2

$$\chi^2 = \sum_{ij} \frac{1}{\sigma_{ij}^2} r_{ij}^2 \tag{5}$$

reaches a minimum. Once the parameters in **C** are optimized, the quality of the fit can be examined in a least-squares projection of the component spectra $\hat{\mathbf{A}}$ onto the data:[43,44]

$$\hat{\mathbf{C}} = (\hat{\mathbf{A}}^{\mathbf{T}}\hat{\mathbf{A}})^{-1}\hat{\mathbf{A}}^{\mathbf{T}}\mathbf{D} \tag{6}$$

The least-squares projected concentration variation derived from the data, $\hat{\mathbf{C}}$, is compared graphically with the optimized time-dependent concentration model, **C**, to examine how the amplitudes of the resolved spectra vary in comparison to the model.

RESULTS AND DISCUSSION

Single-Particle Sampling by Optical Trapping. Optical trapping of single, 5-μm silica particles is readily accomplished. Upon filling the flow cell with the reaction mixture, particles can be captured in the laser focus as they settle onto the coverslip at the bottom of the cell. By adjusting the laser focal spot ~20−30 μm above the coverslip and viewing the sample under white light illumination, the stage can be manipulated in the x,y dimensions to bring a particle into the trap as it settles into focus. Alternatively, it is also possible to trap a particle that has settled and adsorbed to the coverslip by locating the focal spot above the particle and tapping the stage to dislodge the particle from the coverslip surface. This procedure is more difficult for trapping the propylamine-primed silica particles due to the strong electrostatic forces between the aminated silica surface and glass coverslip that can make dislodging the particle from the surface more difficult.

Single particles, once trapped, are levitated above the coverslip surface for analysis. Adjusting the particle height is easily accomplished by simply raising or lowering the microscope objective where optical trapping by the focused laser beam keeps the particle image in the focal plane of the spectrometer. Optical trapping of silica particles is illustrated in Figure 3, where a series of white light images is acquired as a silica particle is levitated from the surface of a coverslip. The first panel (A) is acquired with the focus set in the plane of the coverslip where the particle is resting on the surface. The laser beam is centered in the particle (marked with an arrow), where the reflection of the laser beam from the smooth surface of the coverslip can be observed as an Airy disk pattern. By raising the objective so that the focal plane is 5 μm above the coverslip (B), the particle is levitated and rotated and, the bright reflection of the laser beam from the coverslip is lost. The trapped particle remains in focus while the edges of the two companion particles resting on the coverslip begin to defocus. Clearer evidence of optical trapping is provided by translating the microscope stage ~7 μm (C). This action moves the particles resting on the coverslip while the trapped particle is held in focus by the laser. This result demonstrates the value of optical trapping as a means of stabilizing a particulate sample in space for long-term observation of Raman scattering. Once a particle has been optically trapped, it can then be isolated from other particles and from the coverslip by raising the objective and levitating the particle from the surface. The sequential images in Figure 3D−F show the same silica particle being held at 15-, 30-, and 50-μm distances above the surface. As the height increases, the particles on the coverslip defocus and, at 50 μm, are no longer visible in the bright-field image. At this location, the sample particle is surrounded by solution on all sides, with a 10-particle-diameter space away from the coverslip. This provides free diffusion of reactive molecules into the particle or product molecules out of the particle and into the surrounding solution, which should provide reaction kinetics that are comparable to those for particles dispersed in free solution.

Monitoring Solid-Phase Reaction Kinetics. Confocal Raman microscopy of optically trapped silica particles was used for monitoring reactions in a solid-phase peptide synthesis scheme. The first reaction tested was the addition of fmoc-protected phenylalanine to a propylamine-primed silica surface, the first reaction shown in Figure 2. The time-dependent Raman spectra from the optically trapped aminated particle are shown in Figure 4. The raw scattering data are plotted in the top panel (A) while the spectra in the lower panel (B) are background-corrected by subtracting the first Raman spectrum of the trapped particle so that time-dependent changes can be observed visually. The accumulation of Fmoc-Phe onto the surface is obscured by solvent bands in the raw data from the significant intraparticle pore volume

(40) Draper, N. R.; Smith, H. *Applied Regression Analysis*; John Wiley and Sons: New York, 1981.

(41) Knorr, F. J.; Harris, J. M. *Anal. Chem.* **1981**, *53*, 272−276.
(42) Fister, J. C.; Harris, J. M. *Anal. Chem.* **1995**, *67*, 701−709.
(43) Tauler, R.; Kowalski, B.; Fleming, S. *Anal. Chem.* **1993**, *65*, 2040−2047.
(44) Rivera, D.; Poston, P. E.; Uibel, R. H.; Harris, J. M. *Anal. Chem.* **2000**, *72*, 1543−1554.

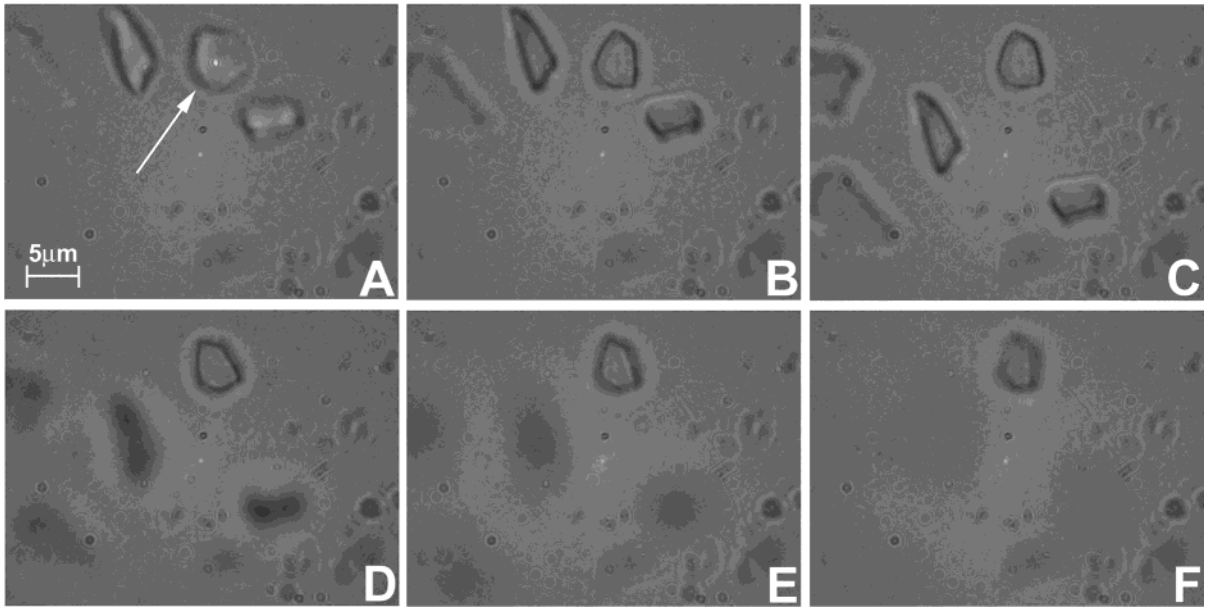

Figure 3. Bright-field images of a single, optically trapped, 5-μm silica particle (arrow). (A) The focused laser spot (bright reflection) is in the plane of the coverslip surface. (B) The focus is raised 5 μm above the coverslip, which traps the particle and eliminates the reflection from the coverslip. (C) Microscope stage is translated ~7 μm and trapped particle remains stationary. (D−F) The focused laser spot is raised 15, 30, and 50 μm above the coverslip surface. Note that the depth of field of these images is ~4 μm,[37] limited by the 0.52 NA of the white light illuminator.

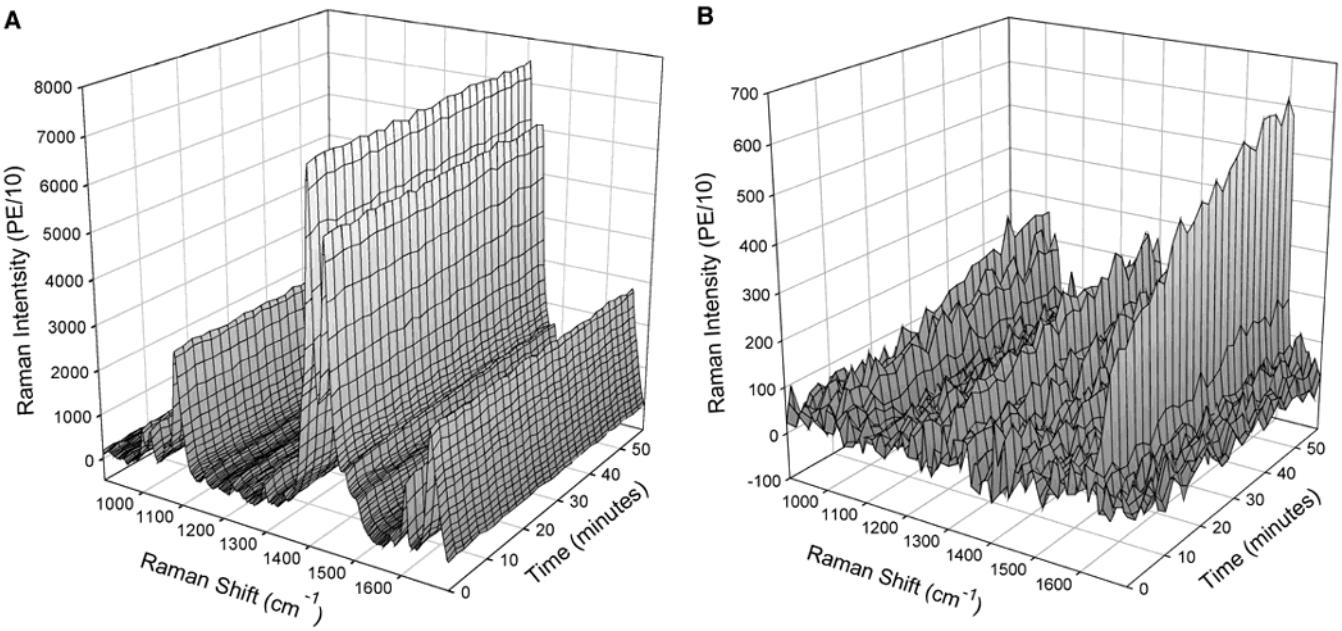

Figure 4. Time-dependent Raman spectra showing Fmoc-Phe addition to a single silica particle. (A) Raw scattering data. (B) Raman spectra background-corrected by subtracting the first spectrum acquired following particle trapping. This subtraction step precludes observing the first particle spectrum and therefore is not used in the data analysis.

(1 mL/g). Background-corrected spectra clearly show the accumulation of Fmoc-Phe scattering intensity, as the ligand binds to the aminated silica surface and its concentration within the particle grows with time.

To determine the rate of the surface binding reaction and to resolve time-dependent Raman spectra into the component contributions, a global least-squares analysis was performed on the raw data in Figure 4A. The accumulation of molecules on the silica surface was fit to an irreversible Langmuir adsorption, characteristic of covalent binding of the ligand to the amine groups on the surface. In the absence of a significant desorption rate, a simple Langmuir reaction model for the rate of occupying surface binding sites is $d\theta/dt = C_o k_b(1 - \theta)$, where C_o is the concentration of molecules in the solution adjacent to the surface, k_b is the rate constant for binding, and $(1 - \theta)$ is the fraction of sites available for binding. Integration of this expression gives a simple exponential rise with a rate that depends on the concentration of molecules in solution:

$$\theta = [1 - \exp(-C_o k_b t)] \quad (7)$$

This Langmuir binding mechanism is a simple model since it

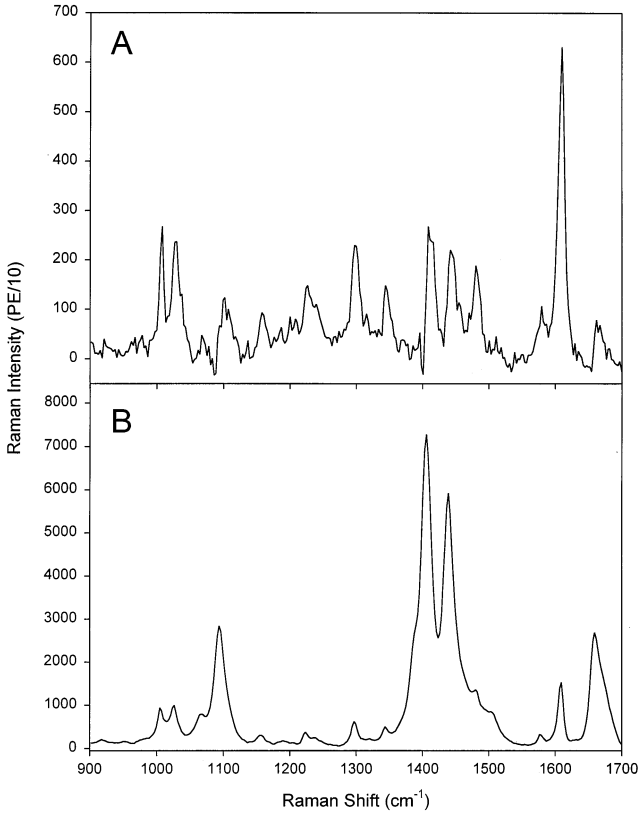

Figure 5. Resolved Raman spectra, **Â**, of components in the Fmoc-Phe addition reaction. (A) Time-dependent spectrum corresponding to Fmoc-Phe binding. (b) Time-independent spectrum corresponding to intraparticle solution components.

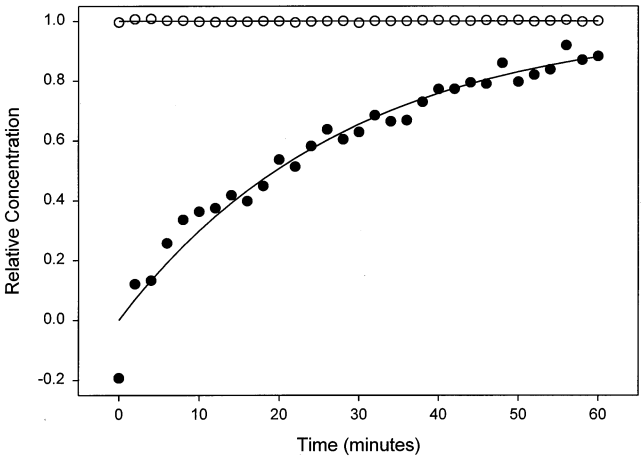

Figure 6. Component concentrations for the Fmoc-Phe addition reaction. The lines represent the model time-dependent behavior of the spectra in **C**, one row of which rises exponentially according to eq 7 and one row is constant. The circles, **Ĉ**, are least-squares projections (Eq 6) of the spectra, **Â**, onto the data.

requires only a single nonlinear parameter, k_b, to be optimized to fit the data. This exponential rise was used as one row vector in constructing the matrix for the time-dependent concentrations, **C**. A second row vector in **C** was constant in time, to account for Raman scattering from solution-phase components that did not vary with time since diffusion from the solution surrounding the particle is efficient on the time scale of the experiment.

This model for the concentrations was applied to the analysis of the uncorrected Raman spectra in Figure 4A, where the two component spectra are resolved by a linear-least squares step as shown in eq 3. The value of the rate constant in eq 7 was varied to achieve a least-squares fit, where the residuals defined by **R** (eq 4) were determined for each value of the rate constant and the sum of the squared residual error χ^2 (eq 5) was minimized. For these data, the reaction rate was 9.0×10^{-4} s^{-1} corresponding to a rate constant, $k_b = 2.1 \times 10^{-2}$ M^{-1} s^{-1}. Using this value of the reaction rate constant in eq 7 gives the time-dependent concentration for one row of the matrix **C**, while a constant vector captures the time-independent intensity in the data. Multiplying the data matrix **D** by the right pseudoinverse of the matrix of model **C** (eq 3) yields a least-squares estimate of the corresponding component Raman spectra, **Â**, which are plotted in Figure 5.

The time-independent spectrum (Figure 5B) corresponds to strong DMF solvent bands and weaker features from the dilute Fmoc-Phe reagent; this spectrum is indistinguishable from the spectrum of the reagent solution. The time-dependent spectrum (Figure 5A) is dominated by bands from the Fmoc-Phe reagent, including the strong in-plane, aromatic C=C stretching mode of the fluorene ring on the fmoc-protecting group at 1609 cm^{-1} [45,46] and the strong symmetric ring-breathing mode of phenylalanine at 1007 cm^{-1}.[47] While this spectrum is dominated by spectral features that derive from the Fmoc-Phe reagent, which accumulates within the trapped particle, there are weak DMF solvent bands, at 1101, 1408, and 1442 cm^{-1}, that are also captured by the time-dependent vector. The presence of these bands is unexpected since the concentration of DMF should decrease within the particle as Fmoc-Phe binds to the surface due to volume displacement. Some increase in solvent band intensity might be due to changes in the local refractive index as aromatic residues accumulate in the particle, increasing the efficiency of light collection. The solvent bands captured by the time-dependent vector, however, have an asymmetric shape that could derive from a frequency shift in the band. Indeed, the peaks of the solvent bands in the time-dependent spectrum are shifted by ~4 cm^{-1} to higher frequency compared to the time-independent spectrum. These shifts could be due to changes in solvent−surface interactions that occur as the reaction proceeds, changing the average band frequencies for the fraction of solvent molecules that interact with the surface of the particle. The time-dependent vector would capture changes in the solvent spectrum that correlate with the reaction at the surface. The shift is especially large (7 cm^{-1}) for the amide NCH bending mode[48] at 1101 cm^{-1}, which should be sensitive to changes in interfacial solvation as fmoc-phenylalanine adds to propylamine groups at the surface.

As a test of the quality of fit of the data to the two time-domain vectors in **C**, the least-squares estimated spectra, **Â**, are projected onto the data[43,44] using eq 6 to obtain least-squares concentrations, **Ĉ**, which is compared graphically with the optimized model, **C**, in Figure 6. The results show that the two spectra in Figure 5 indeed capture both the time-independent and exponentially increasing time dependence in the data. Residual differences between the spectral projections and the model are random except for the first time point, where a negative amplitude is observed

(45) Bree, A.; Zwarich, R. *J. Chem. Phys.* **1968**, *51*, 3, 912−920.
(46) Cuff, L.; Kertesz, M. *J. Phys. Chem.* **1994**, *98*, 12223−12231.
(47) Rava, R. P.; Spiro, T. G.; *J. Phys. Chem.* **1985**, *89*, 1856−1861.

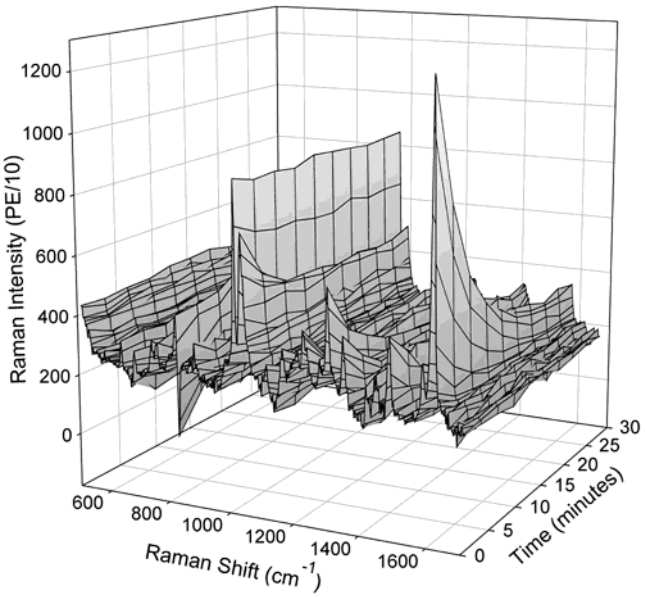

Figure 7. Time-dependent Raman spectra of Fmoc being cleaved from phenylalanine bound to a single silica particle. A particle-free solution spectrum is subtracted from all the data.

for the Fmoc-Phe component, while the amplitude of the solution spectrum is consistent with the other points in time. Subtracting the solution background from the first measured spectrum indeed shows negative spectral amplitude in prominent Fmoc-Phe bands but no residual amplitude for the solvent bands. These results indicate that the *initial* Fmoc-Phe reagent concentration in the center of the particle is probably *lower* than in the bulk solution. The transport of Fmoc-Phe into the particle interior may be initially be slowed due to adsorption; adsorption-inhibited transport of reagents into sol−gel silica pores has been reported to influence the initial kinetics of binding silane reagents to their surfaces.[49]

The kinetic reproducibility of the reaction was also tested for a series of different particles by fitting the increase in intensity at 1609 cm^{-1} to an exponential rise of eq 7. The average rate constant for the reaction for six experiments was found to be $k_b = 2.5 \times 10^{-2}$ M^{-1} s^{-1} with a relative standard deviation of ~40%. The somewhat large deviations in rate may reflect contributions from particle-to-particle variation in the kinetics. Further experiments are ongoing to address this question.

The second step in the reaction scheme, the removal of the Fmoc protecting group from the attached phenylalanine, was also monitored on optically trapped silica particles by confocal Raman microscopy. The solvent background-corrected, time-dependent Raman spectra acquired during this reaction are plotted in Figure 7. Several of the Fmoc bands, including the strong in-plane, aromatic C═C stretching mode at 1609 cm^{-1}, can be observed to decrease during the course of the reaction as the protective group is cleaved from phenylalanine and diffuses out of the particle and into the surrounding solution. Phenylalanine bands, such as the strong symmetric ring-breathing mode at 1007 cm^{-1}, remain at constant intensity during the course of the reaction, showing that the reaction with the piperidine reagent does *not* lead to loss of phenylalanine from the silica surface.

To determine the rate of the Fmoc-deprotection reaction and to resolve the Raman spectra into the component contributions, a least-squares analysis was performed on the data in Figure 7. The cleavage of the Fmoc-protective group from the immobilized phenylalanine was fit to a simple first-order decay model that assumes that the reaction rate remains constant, independent of the fraction of bound groups remaining on the surface: $d\theta/dt = -k_d\theta$, where k_d is the first-order rate constant for deprotection and θ is the fraction of Fmoc molecules remaining on the surface. Integration of this expression gives a simple exponential decay:

$$\theta = \exp(-k_d t) \tag{8}$$

This exponential decay of the fraction of Fmoc bound was used as one row vector in constructing the matrix for the time-dependent concentrations, **C**. A second row vector in **C** was constant in time, to account for Raman scattering from groups that remain on the particle surface and do not vary with time.

This model for the concentrations was applied to analysis of the spectra in Figure 7, where the component spectra are resolved by linear least squares. The value of the rate constant in eq 8 was varied to achieve a least-squares best fit as described above, where the sum of the squared residual error χ^2 was minimized. For the data in Figure 7, the rate constant for deprotection was found to be $k_d = 2.9 \times 10^{-3}$ s^{-1}. Using this result of the reaction rate constant in eq 8 gives the time-dependent concentration for one row of the matrix **C**, while a constant vector captures the time-independent intensity in the data. Multiplying the data matrix **D** by the right pseudoinverse of the matrix of model **C** gives a least-squares estimate of the corresponding component Raman spectra, $\hat{\mathbf{A}}$, which are plotted in Figure 8.

The component spectra show a clean separation of the time-dependent spectral features from the Fmoc-protective group (A) and time-independent bands from immobilized phenylalanine (B). The lack of overlap between the component spectra shows that cleavage of the amide bond of the Fmoc group is highly selective with no loss of phenylalanine intensity during the reaction. The resolved spectra correspond to functional groups present in the separated reaction products. Characteristic peaks from the fluorene ring appear in Figure 8A, including the strong in-plane, aromatic C═C stretching mode at 1609 cm^{-1} [45,46] and in-plane CH bending at 1029 cm^{-1}.[50] In the resolved spectra, this band frequency can be distinguished from the in-plane CH bending of phenylalanine, which appears at 1031 cm^{-1} in Figure 8B. The strongest band in the surface-bound phenylalanine is the symmetric ring-breathing mode[47] at 1007 cm^{-1}.

To test the quality of fit of the two time-domain vectors in **C** to the data, the least-squares estimated spectra, $\hat{\mathbf{A}}$, of Figure 8 are projected onto the data[43,44] using eq 8 to obtain least-squares estimated concentration vectors, $\hat{\mathbf{C}}$, that are compared with the optimized model, **C**, in Figure 9. The results show that the component spectra of Figure 8 capture the constant and exponentially decaying time dependence of the data, with no systematic deviations over time. The reproducibility of the reaction rate was also tested for a series of different particles by fitting the decaying

(48) Jao, T. C.; Scott, I.; Steele, D. *J. Mol. Spectrosc.* **1982**, *92*, 1−17.
(49) Rivera, D.; Harris, J. M. *Anal. Chem.* **2001**, *73*, 411−423.
(50) Lin-Vien, D.; Colthup, N. B.; Fateley, W. G.; Grasselli, J. G. *The Handbook of Infrared and Raman Chacteristic Frequencies of Organic Molecules*; Academic Press: San Diego, CA, 1991; pp 277−281.

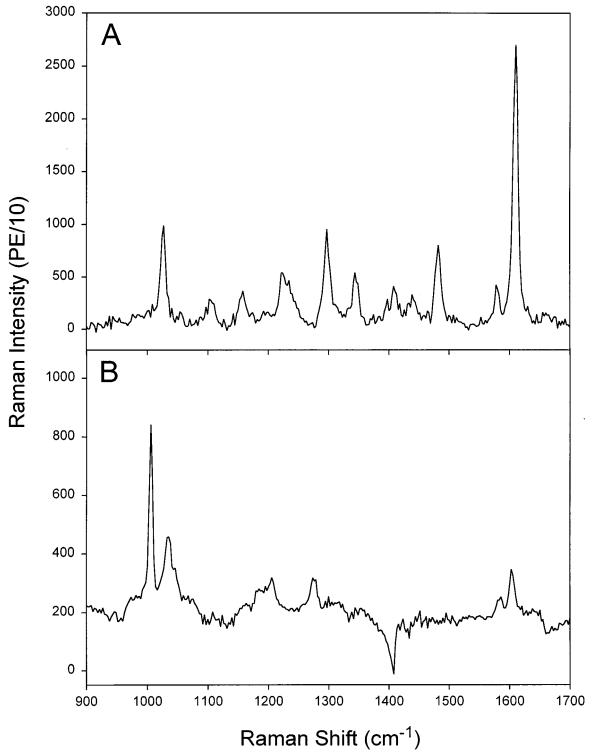

Figure 8. Least-squares resolved Raman spectra, **Â**, for Fmoc removal. (A) Time-dependent spectrum corresponding to the exponential decay of Fmoc from the particle. (B) Time-independent spectrum corresponding to phenylalanine remaining bound to the particle.

intensity at 1609 cm^{-1} to the exponential decay model of eq 8. The average rate constant for the reaction for 10 experiments was found to be $k_d = 2.4 \times 10^{-3}\ s^{-1}$ with a relative standard deviation of ~44%, which is comparable to the variation in the rate observed for the surface binding kinetics, discussed above.

Conclusions. Confocal Raman microscopy can be combined with optical trapping to provide a high-sensitivity method to monitor the kinetics of solid-phase synthesis reactions. The method is capable of monitoring reactions in confocal volumes as small as 2 fL, from as few as 0.8 fmol of scatterers based on the surface coverage by the propylamine primers on the silica. Optical trapping and levitation can be used to move a particle away from the coverslip and into the solution so that reaction conditions

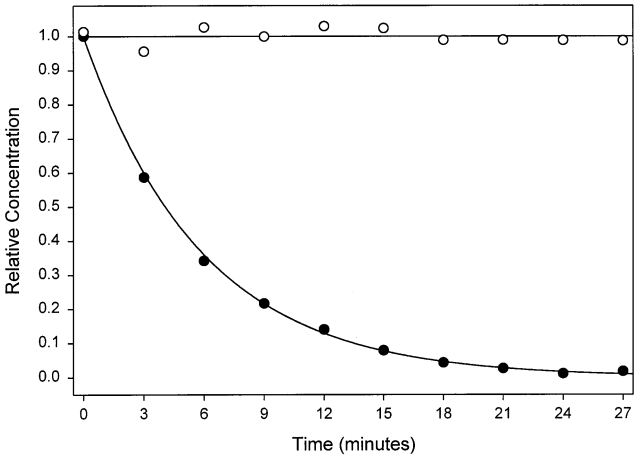

Figure 9. Component concentrations for the Fmoc-Phe addition reaction. The lines represent the model time-dependent behavior of the spectra in **C**, one row of which rises exponentially according to eq 8 and one row is constant. The circles, **Ĉ**, are least-squares projections (eq 6) of the spectra, **Â**, onto the data.

mimic those for dispersed particles. Optical trapping and levitation maintain optical alignment, since the particle is centered laterally along the optical axis and within the focal plane of the objective, where both optical forces and light collection are maximized. Stable, hour-long observations of chemical reactions on individual, trapped silica particles are reported. Using two-dimensional least-squares methods, the Raman spectra collected during the course of a reaction are resolved into their component contributions, allowing the spectra of the time-varying species to be determined, as they bind to or cleave from the particle surface.

ACKNOWLEDGMENT

This research was supported in part by the National Science Foundation under Grant CHE-0137569. Additional support from the University of Utah Research Foundation and the Beckman Foundation (fellowship grant to C.S.S.) are gratefully acknowledged.

Received for review May 14, 2002. Accepted June 28, 2002.

AC020325T